Control of Size and Permeability of Nanocomposite Microspheres

M. S. Toprak,*,† B. J. McKenna,† J. H. Waite,†,‡ and G. D. Stucky*,†,§

Department of Chemistry and Biochemistry, Department of Molecular, Cellular, and Developmental Biology, and Materials Department, University of California, Santa Barbara, California 93106

Received May 5, 2007. Revised Manuscript Received June 19, 2007

This work reports on progress in controlling the size and porosity of spontaneously assembled composite polyelectrolyte microspheres for their potential use in targeted drug delivery applications. In this study, the composite polyelectrolyte microsphere is exemplified by PLK/TSC containing magnetic nanoparticles. The stability of these microspheres against environmental alterations such as pH, ionic strength, and dilution is a critical issue for practical considerations. The effects of ionic strength and dilution on the size of these hybrid spheres were investigated by the addition of salts with different cationic charges and deionized water. Increasing both ionic strength and dilution caused a decrease in the average size of microspheres from ∼700 to ∼200 nm. Ions of +2 charge were observed to screen interactions between the assembling components via a substitution effect. The composite polyelectrolyte microspheres could be mechanically stabilized by cross-linking with glutaraldehyde (GA). The microsphere permeabilities were analyzed using fluorescein-tagged dextran molecules of different MW with confocal laser scanning microscopy and fluorescence recovery after photobleaching. Microsphere permeabilities and critical pore sizes could be controllably decreased by altering the extent of cross-linking, which was monitored by UV−vis spectroscopy. Quantitative analysis revealed that cross-linking can be used to control the diffusion coefficient of dextran and can reduce it by 4 orders of magnitude.

Introduction

Synthesis of organic and inorganic nano- and microspheres has attracted much interest for a variety of applications ranging from drug delivery to chemical storage and catalysis. Magnetic microspheres find widespread and diverse use in many fields, such as environment remediation (removal of toxic and radioactive waste from solutions) and therapeutic[1] (controlled drug targeting,[2] hyperthermia[3]) and diagnostic (ELISA, NMR imaging, sensing) biomedical applications.[4−6] In the field of biomagnetics, microsphere-based technologies play important roles in biosensing;[7] isolation and purification of blood and biomolecules (enzymes, antibodies, peptides, and nucleic acids); separation of biochemical products,[8] cells, bacteria, and viruses from complex biological materials;[9] cell labeling and sorting;[10] and the detection of pathogens.[11] Magnetic microspheres typically are obtained by a variety of techniques such as coating magnetic particles by solvent evaporation,[12] precipitation of iron oxide on polymer microspheres, or heterogeneous polymerization methods, including suspension,[13] dispersion,[14] and emulsion[15] polymerization in the presence of colloidal iron oxide. The first composite magnetic core−shell microspheres were reported by Caruso et al. by the layer-by-layer (LBL) deposition method, for which the shell consists of magnetite nanoparticle/polyelectrolyte multilayers and the colloidal core is a polystyrene latex microsphere.[16,17] Doping of polyelectrolyte capsules with magnetic materials in a controllable way was demonstrated later.[18] Critical parameters to control for such systems for various biological applications include shell biocompatibility, permeability, size control, and mechanical

* Corresponding author. Tel: 805 893-7759. Fax: 805 893-4120. E-mail: mtoprak@chem.ucsb.edu.

† Department of Chemistry and Biochemistry, University of California, Santa Barbara.

‡ Department of Molecular, Cellular, and Developmental Biology, University of California, Santa Barbara.

§ Materials Department, University of California, Santa Barbara.

(1) Tartaj, P.; Morales, M. P.; Veintemillas-Verdaguer, S.; Gonzalez-Carreno, T.; Serna, C. J. *J. Phys. D: Appl. Phys.* **2003**, *36*, R182.
(2) Hafeli, U.; Pauer, G.; Failing, S.; Tapolsky, G. *J. Magn. Magn. Mater.* **2001**, *225*, 73.
(3) Johanssen, M.; Gneveckow, U.; Eckelt, L.; Feussner, A.; Waldöfner, N.; Scholz, R.; Deger, S.; Wust, P.; Loening, S. A.; Jordan, A. *Int. J. Hyperthermia* **2005**, *21*(7), 637.
(4) Neuberger, T.; Schöpf, B.; Hofmann, H.; Hofmann, M.; Von Rechenberg, B. *J. Magn. Magn. Mater.* **2005**, *293*, 483.
(5) Mornet, S.; Vasseur, S.; Grasset, F.; Duguet, E. *J. Mater. Chem.* **2004**, *14*, 2161.
(6) Högemann, D.; Josephson, L.; Weissleder, R.; Basilion, J. P. *Bioconjugate Chem.* **2000**, *11*, 941.
(7) Baselt, D. R.; Lee, G. U.; Natesan, M.; Metzger, S. W.; Sheehan, P. E.; Colton, R. J. *Biosens. Bioelectron.* **1998**, *13*, 731.
(8) Ugelstad, J.; Berge, A.; Ellingsen, T.; Schmid, R.; Nilsen, T.-N.; Mork, P. C.; Stenstad, P.; Hornes, E.; Olsvik, O. *Prog. Polym. Sci.* **1992**, *17*, 87.
(9) Bergemann, C.; Muller-Schulte, D.; Oster, J.; Brassard, L. A.; Lubbe, A. S. *J. Magn. Magn. Mater.* **1999**, *194*, 45.
(10) Chemla, Y. R.; Crossman, H. L.; Poon, Y.; McDermott, R.; Stevens, R.; Alper, M. D.; Clarke, J. *Proc. Natl. Acad. Sci. U.S.A.* **2000**, *97*, 14268.
(11) Megens, M.; Prins, M. *J. Magn. Magn. Mater.* **2005**, *293*, 702.
(12) Ramanujak, R. V.; Chong, W. T. *J. Mater. Sci. Mater. Med.* **2004**, *15*, 901.
(13) Yang, C.; Liu, H.; Guan, Y.; Xing, J.; Liu, J.; Shan, G. *J. Magn. Magn. Mater.* **2005**, *293*, 187.
(14) Horák, D.; Semenyuk, N.; Lednicky, F. *J. Polym. Sci., Part B: Polym. Chem.* **2003**, *41*, 1848.
(15) Kondo, A.; Kamura, H.; Higashitani, K. *Appl. Microbiol. Biotechnol.* **1994**, *41*, 99.
(16) Caruso, F.; Susha, A. S.; Giersig, M.; Möhwald, H. *Adv. Mater.* **1999**, *11*, 950.
(17) Caruso, F.; Spasova, M.; Susha, A.; Giersig, M.; Caruso, R. A. *Chem. Mater.* **2001**, *13*, 109.
(18) Shchukin, D. M.; Radtchenko, I. L.; Sukhorukov, G. B. *Mater. Lett.* **2003**, *57*, 1743.

10.1021/cm071215b CCC: $37.00
Published on Web 07/26/2007

stability. Improvement and tailoring of the mechanical properties of these types of polyelectrolyte microcapsules by glutaraldehyde cross-linking was recently reported by Möhwald et al.[19]

In biological applications, the effectiveness of microparticulate materials can be highly improved if they can act simultaneously as carriers for biologically active molecules. In this sense, porous materials are advantageous, because they present additional surface area, which strongly influences the obtainable loading capacity and release rates. Various strategies are used for the fabrication of porous polymeric and composite microspheres. Particulate resins are conventionally synthesized via suspension polymerization involving a complex combination polymerization, cross-linking, phase separation, and microgel formation, microgel fusion, and pore in-filling. Porosity was introduced by using an oil-in-water emulsion evaporation technique and subsequent treatment in a fluidized bed reactor to close off the pores.[20] Porous microspheres have also been synthesized via self-assembly of monodisperse polymer nanospheres, which eliminates multistep processing.[21] A dense, aqueous emulsion of nanospheres was dispersed as microdroplets in a continuous oil phase, followed by removal of water.

Interaction with biological systems requires a stable, biocompatible microsphere surface. The microsphere size should also be tailorable for a variety of applications. Furthermore, for drug delivery applications, porosity and permeability control are important. In this work, we present a route for the formation of MNP containing nanocomposite microspheres with adjustable size, tailored to have different critical pore size and permeability by controlling the cross-link density. This study reveals a route to optimize cross-linking to encapsulate macromolecules within a selected size range, thus providing an important functionality for drug delivery applications.

Experimental Section

Chemicals. $FeCl_2 \cdot 4H_2O$, $FeCl_3 \cdot 6H_2O$, NH_4OH, HCl, poly-L-lysine, (PLK 67 kDa), trisodium citrate (TSC), FITC-Dextran with different MW (4, 10, 20, 40, 70, and 250 kDa), NaCl, $CaCl_2$, and $MgCl_2$ were obtained from Sigma-Aldrich. Glutaraldehyde and glycine were obtained from Ted Pella Inc., CA. All chemicals were used as received and aqueous solutions were prepared by dissolving the corresponding chemicals in DI water, 18 MΩ.

Surface-Modified Magnetic Nanoparticles. Superparamagnetic nanoparticles were prepared using a previously described procedure.[22] In a typical process, a mixture of Fe^{2+} and Fe^{3+} was hydrolyzed with NH_3 solution at pH >10 in an oxygen-free atmosphere. Afterward, the reaction mixture was heated to 80 °C under an Ar flow, followed by the addition of TSC.[23] Subsequently, the reaction mixture was cooled and magnetic nanoparticles (MNPs) were collected by applying an external magnetic field.

Hybrid Coacervate Formation and Cross-Linking. Poly-L-lysine (PLK) was dissolved in deionized water to 2 mg/mL. A solution of magnetic nanoparticles (MNP) having a net negative surface charge was mixed with a chosen amount of PLK solution, upon which the solution turned cloudy. A typical sample was fabricated by mixing 20 μL of 2 mg/mL PLK solution with 120 μL MNP (1.6 mg/mL TSC). The reaction was mixed vigorously for 15 s using a vortex mixer.

Effect of Ionic Strength and Dilution. The effect of ionic strength was investigated using salts with different ionic charges; namely NaCl, $CaCl_2$, and $MgCl_2$. Stock solutions of these salts at 50 mM concentration were prepared and added to PLK solution prior to mixing with TSC.

The effect of dilution was investigated in a similar way, by adding different volumes of DI water to PLK solution prior to mixing with TSC.

All samples were cross-linked, after 3 min of aging, by the addition of 120 μL of 2.5 wt % GA,[24] the excess of which was quenched by the addition of glycine after the desired cross-linking period.

Particle Size Analysis. Particle size analysis was performed on several SEM micrographs counting a minimum of 150 cross-linked microspheres. Size distribution plots are presented using the average nanocomposite sphere size with one standard deviation, $d_{ave} \pm SD$.

Incubation Tests. After spontaneously assembled composite microspheres were cross-linked for different durations, they were collected by centrifugation and then redispersed in DI water. FITC-dextran solutions with different MWs were then added in 20 μL (~2 mg/mL) portions to 100 μL of these composite microspheres. After 5 min of incubation/equilibration time, the samples were transferred to glass slides and analyzed by confocal laser scanning microscopy (CLSM).

Quantification of Diffusion Coefficient/Permeability. The microsphere permeability was quantified by means of fluorescence recovery after photobleaching (FRAP) using FITC-dextran as a molecular probe. To follow the diffusion of FITC-dextran into the microsphere, the microsphere's interior was photochemically bleached with the CLSM ArKr laser (488 nm), at 100% intensity, for sufficient durations. Imaging was typically performed at about 4% of the maximal laser intensity. The interval between image scans varied, depending on recovery rates established in preliminary experiments. Recovery was considered complete when the intensity of the photobleached region plateaued. For quantitative analysis, the fluorescence intensity signals within closed circular areas were averaged to yield intensity values for each interval.

Results and Discussion

Hybrid coacervates are formed by the addition of MNP-citrate solution into the PLK solution by way of coulombic interactions between the positively charged (free) amine groups of PLK and the negatively charged carboxyl groups on the nanoparticles (Figure 1a). Coacervation is a dynamic process, and these interactions can be easily disturbed by various factors. In our earlier report, we investigated the effect of various parameters on these hybrid microspheres and identified the charge ratio of polyelectrolytes, aging time, temperature, and PLK MW as critical parameters for the size control.[25] Although fine control of size was achieved, further control of the properties of the microspheres by the manipu-

(19) Tong, W.; Gao, C.; Möhwald, H. *Chem. Mater.* **2005**, *17*, 4610.
(20) Kim, H. K.; Chung, H. J.; Park, T. G. *J. Controlled Release* **2006**, *112*, 167.
(21) Mouaziz, H.; Lacki, K.; Larssonb, A.; Sherrington, D. C. *J. Mater. Chem.* **2004**, *14*, 2421−2424.
(22) Turinho, F. A.; Franck, R.; Massart, R. *Prog. Colloid Polym. Sci.* **1989**, *79*, 128.
(23) Deng, Y.; Yang, W.; Wang, C.; Fu, S. *Adv. Mater.* **2003**, *15*, 1729.
(24) Walt, D. R.; Agayn, V. I. *TrAC, Trends Anal. Chem.* **1994**, *13*, 425.
(25) Toprak, M. S.; McKenna, B. J.; Waite, J. H.; Stucky, G. D. *Adv. Mater.* **2007**, *19*, 1299.

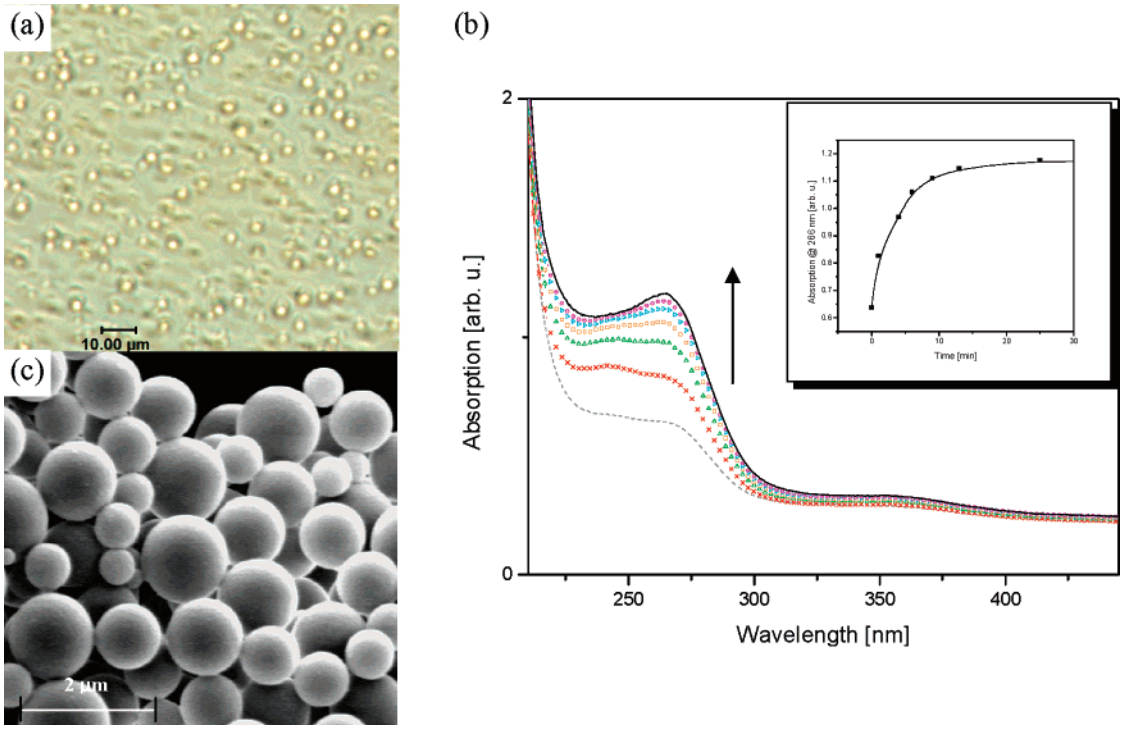

Figure 1. (a) Optical micrograph of as-prepared magnetic coacervates; (b) UV−vis spectra of PLK−MNP coacervates cross-linked with 2.5 wt % GA for different durations: 0, 1, 4, 6, 9, 13, and 25 min, from bottom to top. The inset shows the absorption due to newly formed imide (−C═N−) bonds at 266 nm as a function of time; (c) SEM micrograph of cross-linked magnetic microspheres.

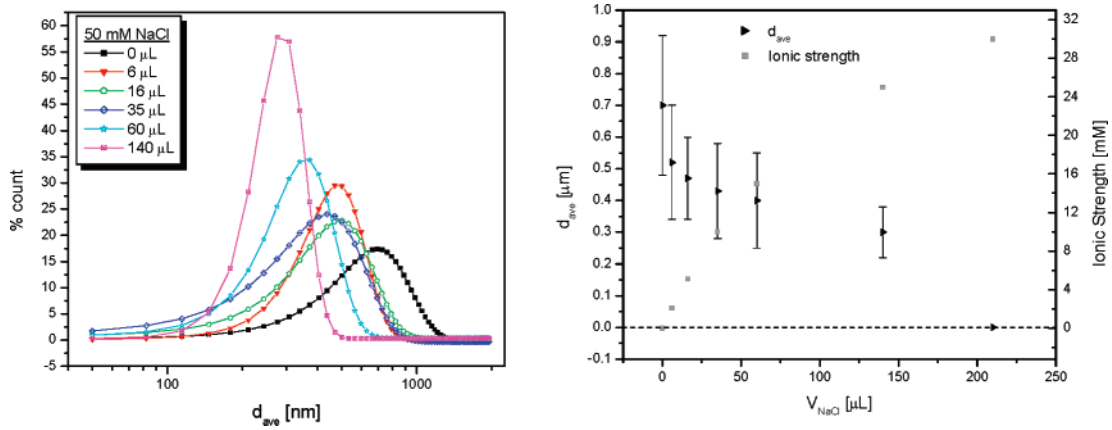

Figure 2. Effect of adding aliquots of 50 mM NaCl on the average hybrid microsphere diameter and solution ionic strength. Error bars indicate one standard deviation.

lation of other physical parameters such as ionic strength, pH, and dilution was sought. The extent of coacervation decreases significantly with a decrease in ionization. For example, we have found that a deviation of ±1 unit from the pI of the polyelectrolyte leads to loss of the coacervate as the charge densities in the polyelectrolytes, and their interactions, become weaker.

The effect of ionic strength on the size of resultant hybrid coacervates/micropsheres was investigated by using salts of +1 and +2 charged cations (Figures 2 and 3). The average size was observed to decrease with increasing ionic strength, achieved by adding equal portions of different salts. In the case of NaCl addition, the average microsphere size was reduced from 700 nm under original reaction conditions to 300 nm at 25 mM added ionic strength (Figure 2). No hybrid sphere formation was observed above 25 mM ionic strength for NaCl. In the case of $CaCl_2$, the average size decreased from 700 to 350 nm with an added ionic strength of 6 mM, above which no spherical formations were observed, shown in Figure 3. We attribute the decrease in the average size to the electrostatic screening of polyelectrolytes by the increasing ionic strength. The significant difference in responses to these two different salts is attributed to complexation of Ca^{2+} with citrate ions, impeding the spontaneous assembly. When Ca^{2+} ions were replaced with Mg^{2+} ions, no spherical assemblies were observed at any ionic strength conditions. This greater activity of Mg^{2+} is attributed to its much larger hydrated radius (ca. 4× larger than hydrated Ca^{2+}), which causes a siginificant shielding of citrate ions, thus interfering even more with the spontaneous assembly process.[26]

The effect of dilution on the average size of hybrid microspheres was similar to that observed for increasing ionic

(26) Maguire, M. E.; Cowan, J. A. *BioMetals* **2002**, *15*, 203.

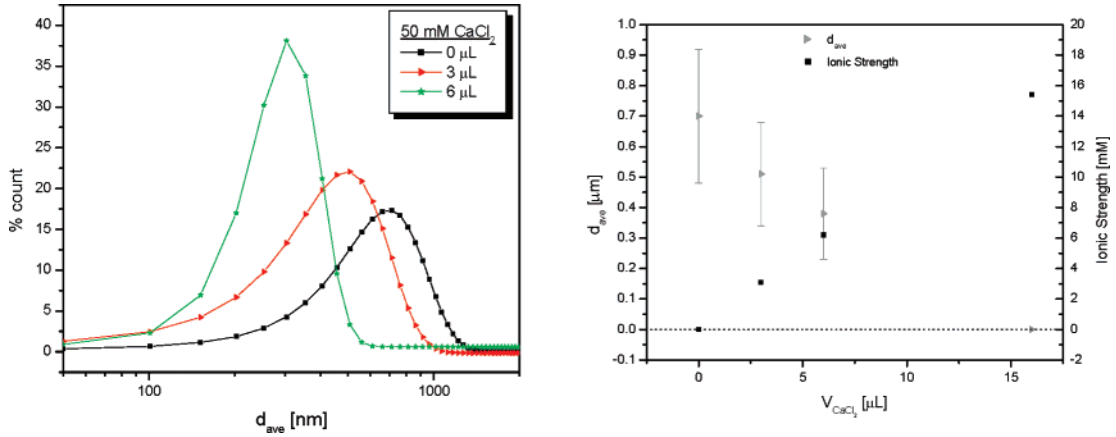

Figure 3. The effect of adding aliquots of 50 mM $CaCl_2$ on the average hybrid microsphere diameter and solution ionic strength. Error bars indicate one standard deviation.

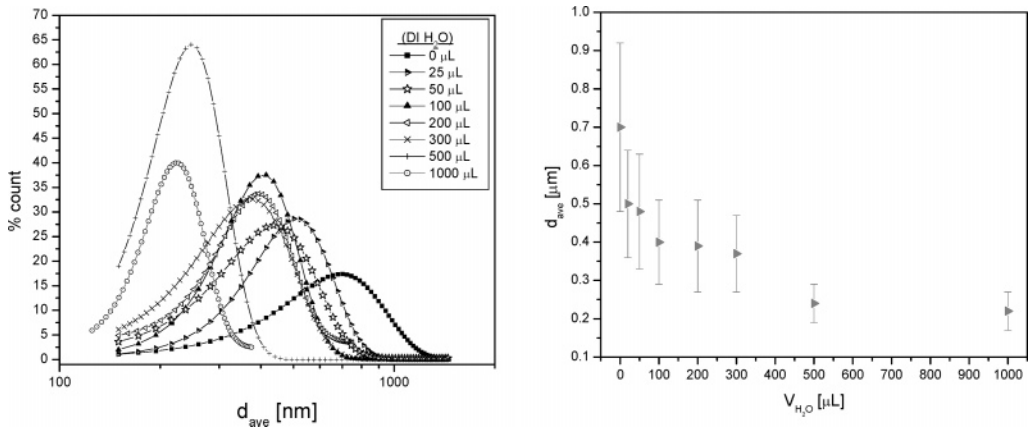

Figure 4. Diameter distributions of hybrid microsphere samples at different dilutions, as calculated from SEM micrographs. Error bars indicate one standard deviation.

strength and is presented in Figure 4. Dilution increased the distance between charged species making their interaction less probable, hence resulting in an increased number of nucleation sites of hybrid microspheres of reduced size.

Mechanical stability of the assemblies at various pH environments and ionic strengths is essential for their potential as drug delivery devices. Mechanical stability was achieved by cross-linking with glutaraldehyde (GA). This forms -C═N− bonds (Schiff bases), which absorb in the UV region.[27] Therefore, UV−vis spectroscopy was used to monitor the cross-linking as well as the extent of GA grafting onto PLK and is shown in Figure 1b. The broad absorption in the UV region increased with treatment time, indicating an increase in the number of -C═N− bonds. The absorbance at 266 nm as a function of time is shown in the inset, demonstrating a very quick initial reaction that gradually slows. Therefore, the degree of cross-linking can be tuned by selecting a reaction time and quenching with glycine to suppress further reaction. An SEM micrograph of cross-linked hybrid microspheres is presented in Figure 1c.

Fluorescence emission data were collected following 488 nm excitation and are presented in Figure 3 for samples at different processing stages. As control experiments, non-cross-linked hybrid coacervates and crosslinked PLK were analyzed (Figure 5a). Coacervate solutions with magnetic nanoparticles alone showed an emission band centered at 520 nm, which was also observed for a suspension of magnetite nanoparticles. Cross-linked magnetic microspheres showed an emission band around 550 nm, as did cross-linked PLK; therefore, this band was assigned to the emission from imide (−C═N−) bonds formed during the cross-linking. Emission of magnetite entrapped within microspheres was not resolvable, probably because of exciton transfer to PLK. The emission of FITC-labeled dextran was centered at 520 nm, Figure 5b, but increasing amounts of FITC-dextran in microsphere solutions enhanced an emission band with a slightly blue-shifted center at 510 nm, a result of interaction with the reaction medium. Importantly, this analysis indicates the proper wavelengths for resolving signals of imide bonds and FITC: FITC detection was performed in the range 510−530 nm, whereas the cross-linked microspheres were detected in the range of 540−570 nm.[28]

Tailoring of the microspheres' porosity was controlled by the duration of the cross-linking treatment. On the basis of the data obtained, Figure 1b, samples were cross-linked for 1 min or longer periods to fabricate microspheres with different pore sizes and permeabilities. FITC-tagged dextran

(27) Tong, W.; Gao, C.; Möhwald, H. *Chem. Mater.* **2005**, *17*, 4610.

(28) Toprak, M. S.; McKenna, B. J.; Waite, J. H.; Stucky, G. D. In *Heterogenous Integration of Materials for Passive Components and Smart Systems*; Nino, J. C., Roozeboom, F., Muralt, P., Troiler-McKinstry, LaVan, D., Eds.; Material Research Society Symposium Proceedings Vol. 969; Materials Research Society: Warrendale, PA, 2007; p 0969-W03-11.

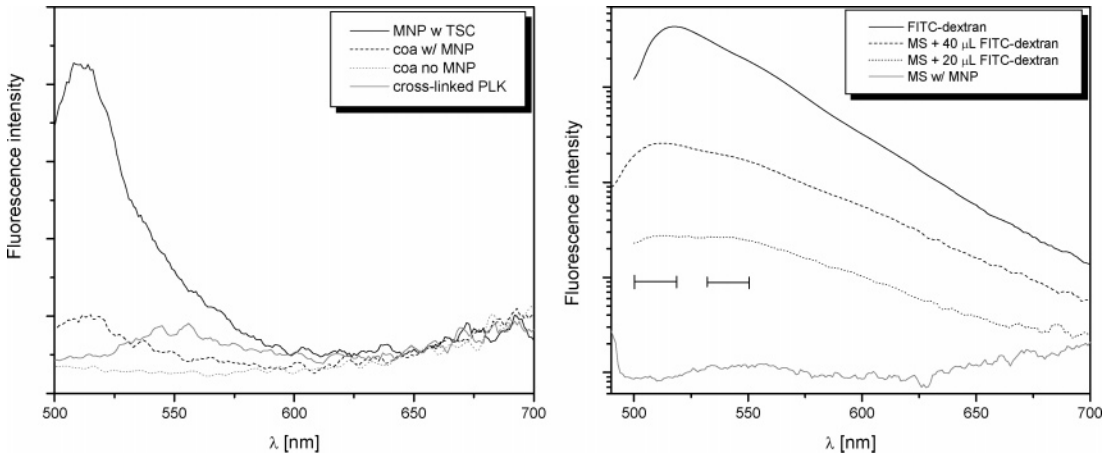

Figure 5. Fluorescence emission of hybrid microspheres at different processing stages.

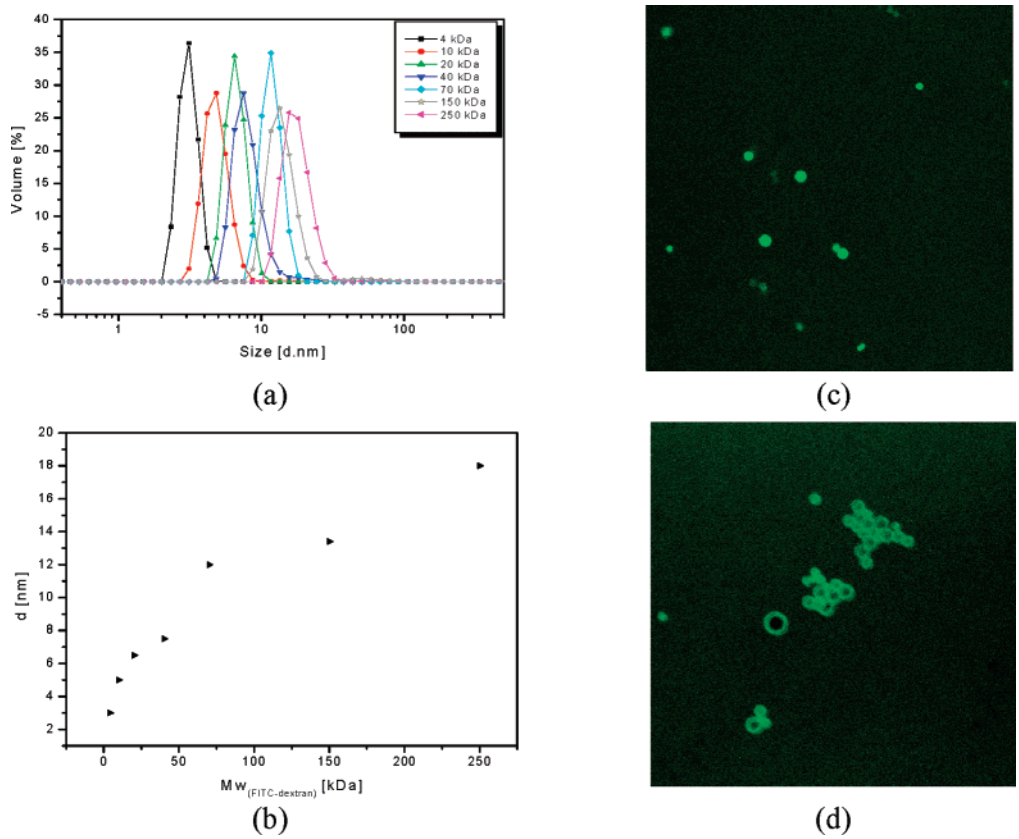

Figure 6. (a) Hydrodynamic size distribution of FITC-dextran molecules with different MWs; (b) average size of FITC-dextran molecules with different MWs; Confocal microscopy images of hybrid microspheres that are (c) permeable and (d) impermeable to FITC-dextran.

molecules were added into the microsphere suspension and the system was allowed to equilibrate for 5 min prior to analysis. Confocal microscopy was then performed to determine to what extent FITC-dextran molecules were impregnated into the variably cross-linked microspheres. The hydrodynamic size distribution of the various FITC-dextran molecules is presented in Figure 6a; the average hydrodynamic size increased with MW, as expected (Figure 6b).

Thirteen samples of microspheres were prepared with different levels of cross-linking. The extent of cross-linking was determined by monitoring the UV absorption intensity as presented in Figure 2b, inset. More specifically, how the degree of cross-linking affected permeability of these nanocomposite microspheres was tested with samples cross-linked for durations of 1, 2, 3, 5, 8, 12, 16, 24, and 33 min and 1, 3, 24, and 48 h. The results are summarized in Table 1 under three categories: (i) permeable to FITC-dextran, as shown by complete filling of the micropsheres in Figure 6c; (ii) impermeable to dextran, such that negatively charged FITC-dextran molecules are adsorbed only on the microsphere surfaces, as shown in Figure 6d; and (iii) critically permeable, for samples in which both (i) and (ii) are observed. These observations show that porosity of these composite microspheres could be successfully tailored by an adjustable and measurable cross-linking treatment.

The two shortest durations of cross-linking, 1 and 2 min, resulted in the largest pores and permitted entry to FITC-dextran molecules with a hydrodynamic radius of 18 nm (250 kDa). Prolonged cross-linking for 3 and 5 min reduced the critical pore size and allowed the diffusion of molecules with

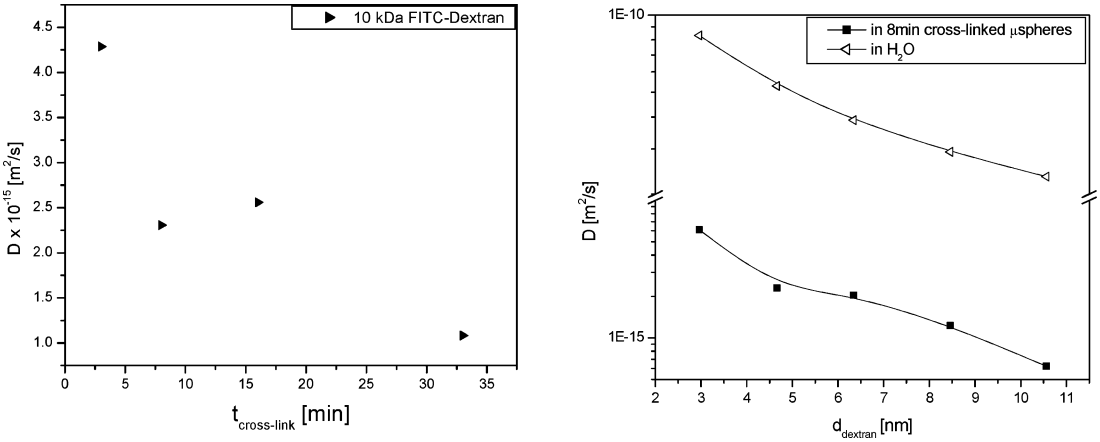

Figure 7. Diffusion coefficients calculated from FRAP experiments for (a) 10 kDa FITC-dextran diffusing into microspheres cross-linked for different durations, and (b) dextran molecules with different MWs diffusing into 8 min cross-linked microspheres.

Table 1. Permeability of Hybrid Microspheres, Cross-Linked (CL) for Different Durations, to FITC-Dextran Molecules with Different MWs

CL Duration	FITC-dextran with different MWs						
	4 kDa	10 kDa	20 kDa	40 kDa	70 kDa	150 kDa	250 kDa
t=1 min							
t=2 min							
t=3 min							
t=5 min							
t=8 min							
t=12 min							
t=16 min							
t=24 min							
t=33 min							
t=1 hr							
t=3 hr							
t=24 hr							
t=48 hr							

Permeable Critical permeability Impermeable

about 12 nm hydrodynamic radius. When the cross-linking treatment was extended to 8 min, the critical pore size reduced to under 12 nm. Cross-linking for 12 min resulted in pores of around 8 nm. Extended periods of cross-linking (between 16 min and 48 h) resulted in microspheres with similar porosities, all permeable to molecules with an average hydrodynamic radius of 5 nm. As expected, the longest duration of cross-linking in this series resulted in the smallest pore size. Pore sizes did not change significantly for samples cross-linked beyond 16 min, despite an increasing UV absorption peak. This suggests that some of the GA molecules coupled to PLK did not function as cross-linkers, even though they formed Schiff bases.

Excess fluorescein-labeled dextran was added into the medium and fluorescence recovery after photobleaching (FRAP) was performed with procedures established in the literature.[27−30] Diffusion of FITC-dextran molecules into the microspheres was monitored with time to generate a fluorescence recovery curve. The fluorescence recovery for these solid microspheres, for times after 40% recovery, can be approximated as

$$C(t) = \pi R_o^2 C_o \left[1 - \frac{8}{\pi^2} e^{-tD(\pi/R_o)^2}\right] \quad (1)$$

where $C(t)$ and C_o denote the fluorescence/concentration at time t and $t = 0$, respectively. D is the diffusion constant, and R_o is the radius of the microsphere. The fluorescence recovery curves for different samples of known cross-sectional areas were fit to calculate the diffusion coefficients of FITC-dextran molecules into composite microspheres of different cross-linking durations.

The diffusion coefficients of FITC-dextran molecules of different MWs into crosslinked microspheres were on the order of 1×10^{-15} m^2/s (See plot in Figure 7a), which is about 4 orders of magnitude smaller they are in water, mainly because of the cross-linking process. Furthermore, a series of FRAP experiments were performed with 10 kDa FITC-dextran molecules infiltrated into microspheres cross-linked for various durations. Diffusion coefficients calculated for FITC-dextran molecules within these microspheres are presented in Figure 7b and showed a trend of decreasing D with greater cross-linking. Hence, cross-links reduced pore sizes and restricted the free movement of FITC-dextran molecules. These results suggest that the diffusion of macromolecules through the nanocomposite network can be controlled by their sizes relative to those of the microsphere pores.

Conclusions

These studies demonstrate that properties of functional composite microspheres, cooperatively assembled via com-

(29) Ibarz, G.; Dähne, L.; Donath, E.; Möhwald, H. *Chem. Mater.* **2002**, *14*, 4059.
(30) Ibarz, G.; Dähne, L.; Donath, E.; Möhwald, H. *Macromol. Rapid Commun.* **2002**, *23*, 474.

plex coacervation, can be tailored by modifying the conditions during and/or after the assembly step. Their size can be adjusted by a proper control of the ionic strength and amount of dilution in the synthesis medium, in addition to previously reported parameters such as temperature, aging time, polymer MW, and charge ratio. The mechanical stability and porosity of the composite microspheres, exemplified here using PLK/TSC microspheres with magnetic nanoparticles, can be tailored by glutaraldehyde (GA) cross-linking, the extent of which can be monitored by UV−vis spectroscopy. Cross-linking decreased microsphere permeabilities and resulted in smaller critical pore sizes. FRAP experiments performed using FITC-dextran molecules of various MW revealed that cross-linking could control microsphere permeabilities and that the dextran diffusion coefficients decreased by 4 orders of magnitude. These results are of critical importance for the design of functional microspheres that can control diffusion on the basis of size selection, or for entrapment of molecules of a chosen size while allowing free transfer of smaller molecules. Although PLK and MNPs with citrate were featured here as a case study, the design principles and synthetic methods are applicable to a variety of polyamines and nanoparticles appropriately functionalized at their outer surfaces. The facile assembly and tunability of properties supports the widespread applicability of these nanocomposites as magnetically functionalized drug delivery devices.

Acknowledgment. The fellowship for M.S.T. from the Knut and Alice Wallenbergs Foundation is thankfully acknowledged (UAW2004.0224). This research was supported in part by the Public Health Service/NIH under Grant R01 DE 014572 and by the National Science Foundation under Grant DMR02-33728. This work made use of MRL Central Facilities supported by the MRSEC Program of the National Science Foundation under Award DMR05-20415. We are also thankful to Prof. Zasadzinski and Mr. Patrick C. Stenger for their help and for granting us access to their confocal microscopy facilities.

CM071215B